MINAR International Journal of Applied Sciences and Technology
ISSN: 2717-8234
Article type: Research Article

Received: 18/10/2022 **Accepted:** 01/11/2022 **Published:** 01/12/2022

NUMERICAL INVESTIGATION OF A HIGH-TEMPERATURE ENERGY STORAGE

Afrah Turki AWAD [1]

Imam Ja'afar Al-Sadiq University, Iraq

Kamal Jalal Tawfeeq ALBAZZAZ

Imam Ja'afar Al-Sadiq University, Iraq

Abstract

Nitrate solar salt had been analyzed as a storage medium for the applications of the high-temperature solar energy storage system. The numerical investigation of the storage system would save time, cost, and effort. In this study, a simulation study using ANSYS CFX software was utilised. This study was validated against an experimental setup, which was designed for heat transfer study of storage material. An Ansys-CFX code that is built and developed to simulate the phase change material (PCM) inside the storage system, was presented. The developed model was validated against experimental data using the same dimensions of the storage system and the same storage material (Case 1 was PCM (only nitrate solar salt; KNO3: NaNO3 by 40:60 molar ratio) and case 2 was nano-PCM (0.5 wt.% Fe2O3+ nitrate solar salt)). This validation ensured the feasibility of using CFD as a design tool. According to Ziskind (2021), the enthalpy porosity techniques can be defined as apparent analogy between the liquid state of PCM inside the mushy zone and the following fluid flow into a porous medium. This techniques had been implemented in the CFX code to show the charging process of the phase change material. It was shown that the natural convection effect was presented in the liquid phase during the charging process. In addition, nano-PCM shows an improvement of charging process by 17.021%. According to the transient temperature measurements, it was found that there was a good match between the experimental data and the data from the CFX code with error less than 5%.

Keywords: CFX Code, Simulation Study, Improved Heat Transfer, Charging Processes, High-Temperature Solar Energy Storage System.

http://dx.doi.org/10.47832/2717-8234.13.12

[1] afrah.turki@sadiq.edu.iq

I. INTRODUCTION

The thermal energy storage (TES) is an important factor to reduce peak power demand. The phase change material (PCM) has been widely used to store the energy in the TES system. PCM can be used to increase the efficiency of the TES. PCM has been used over the past 37 years [Dermardiros, et. al., 2015]. However, many challenges are remaining. Therefore, many studies are required to overcome these challenges. In fact, the simulation study of the PCM would save the cost, time, and space that would be required to install an experiment. Furthermore, simulation PCM could provide additional insights which could be difficult or impossible, especially for the high-temperature solar energy storage system. Therefore, different studies have been conducted to simulate the PCM using Fluent software. The melting/solidification model follows the enthalpy-porosity method by finite volume method to simulate the phase change of the storage medium in solar energy storage. There are different studies used the enthalpy-porosity method to simulate the PCM in ANSYS-Fluent by many researchers such as Shmueli et al. (2010), Bhaumik (2012), Hossain et al. (2015), Fadl and Eames, (2019), and 2. Yadav et. al., (2022)).

According to the [Fluent manual], the enthalpy porosity model basically relays on the addition of sensible and latent enthalpies.

Furthermore, nanotechnology has been implemented in the TES to improve the performance of the PCM. Therefore, there were simulation studies conducted on the heat transfer of the PCM and nano-PCM. However, these simulation studies were for low-temperature applications (Sebti et al., 2011, Valan et al. 2013, Sharma et al., 2014, Li et. al. 2020, Bouzennada et. al. 2021, Ahmed et. al. 2022, and Abderrahmane et. al. 2022). Ansys-Fluent software is used to show the melting of the PCM or nano-PCM and therefore assess the feasibility of using CFD for design purposes.

It would be advantageous to simulate the storage system for high-temperature applications. Therefore, for the first time, the ANSYS-CFX (version 17.0) has been used to simulate the melting process of the PCM and nano-PCM for TES. In this paper, a code was designed to simulate the melting process of the PCM because the melting/solidification model does not exist in CFX. The expression language of the CFX is flexible which is simple to specify the modeling of the PCM. Therefore, CFX was chosen to design the melting of PCM/nano-PCM. In this paper, the CFX code has been designed for two different cases depending on the type of PCM. Case 1 was PCM (only nitrate solar salt; KNO_3: $NaNO_3$ by 40:60 molar ratio) and case 2 was nano-PCM (0.5 wt.% Fe_2O_3+ nitrate solar salt). Moreover, the design code in CFX has been validated against the Ansys-Fluent code and experimental data.

II. ANSYS SIMULATION

1. Geometry and Meshing:

The 3-D geometry was built using an Ansys workbench-design modeller (version 17.0). Ansys was used to simulate the charging process of PCM in the shell-and-tube solar energy storage system. This simulation was validated against an experimental setup with exact boundary conditions. The shell diameter was 101.4 mm with a thickness of 2 mm. The diameter of the inner pipe was 25 mm. The length of the 3-D geometry was 300 mm. All solid materials were made of stainless steel while the fluid material was PCM.

Two different cases were simulated. In case 1, PCM was nitrate solar salt (60 $NaNO_3$: 40 KNO_3). While in case 2, PCM was nano-PCM (0.5 wt.% Fe_2O_3+ nitrate solar salt) to show the differences between the PCM without nanoparticles and with nanoparticles. Figure (1) shows the geometry.

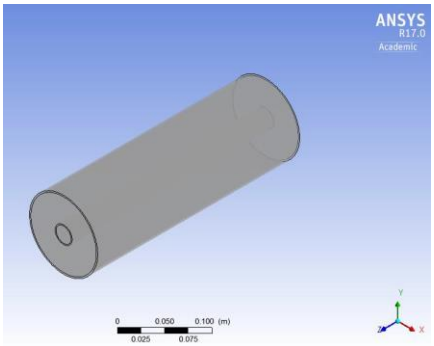

Figure (1) shows the geometry.

The type of mesh was hexahedral with high quality. The aspect ratio tool is used to measure this quality by dividing the length over the height of the cell (Bakker, 2002). The highest value of the aspect ratio (AR up to 1), means the highest quality of the mesh. In our case, the aspect ratio was in the range of 0.9<AR<1, as shown in Figure (2).

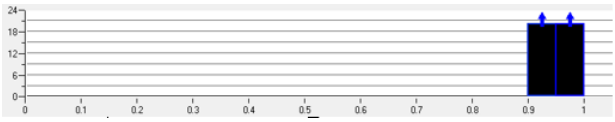

Figure (2) shows the quality of the mesh.

2. Mesh independent study:

The higher number of nodes would consume a longer running time to show the results. In addition, the type of mesh used in the simulation setup has a very big influence on the quality of the work in terms of the stability of the residuals and the convergent.

Therefore, it is better to specify the optimum values of the node and this is called a mesh-independent study. In this paper, four different numbers of nodes were tested, as shown in Table (1). It concluded that increasing the number of nodes (higher than 7942) was not show differences in the results. Therefore, we depended on mesh number 2, as shown in Figure (3).

TABLE 1: SHOWS MESH DETAILS

Details	**Mesh 1**	**Mesh 2**	**Mesh 3**	**Mesh 4**
Elements	4920	5920	6920	439632
Nodes Number	6942	7942	8942	407680

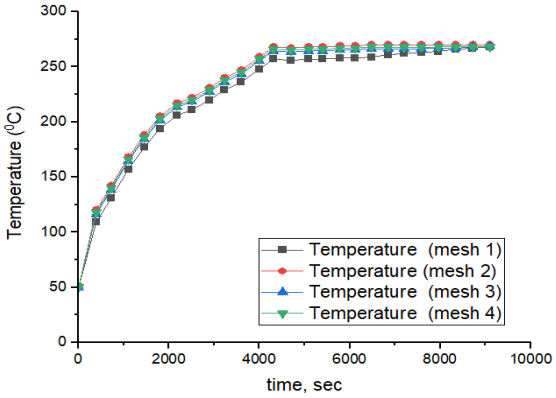

Figure (3) shows a mesh-independent study.

There were no big differences between the results from mesh numbers 2, 3, and 4, as shown in figure (3). Therefore we used mesh number 2 which owns less number of nodes. Because the higher number of nodes required a longer time for running the simulation. Additionally, Tay et. al 2015, mentioned that a small number of nodes should be enough to accurately simulate the PCM. This is in accordance with our results.

3. Boundary conditions

Figure (4) describes the boundary condition on the geometry. In order to ensure similarity with experiments, the top and bottom covers of 3-D geometry assumed like wall boundary conditions with values of heat losses. These heat losses were measured by the film temperatures (Thirumaleshwar, 2009). The heat loss can be calculated by equation (1):

$h = Nu.\ k/Lc$ (1)

$Nu = 0.54\ Ra^{1/4}$ (for $10^4 < Ra < 10^7$) (2)

$Nu = 0.27\ Ra^{1/4}$ (for $10^5 < Ra < 10^{11}$) (3)

Where:

$Ra = [\rho^2.g.\beta.(Ts - T\infty)\ Lc^3\ Pr]/\ \mu^2$ (4)

$Tf = (Ts + T\infty)/\ 2)$ (5)

According to the above equations, h from the top surface = 8.53 W/ (m^2. K). While the value of h from the bottom surface=3.18 W/ (m^2. K).

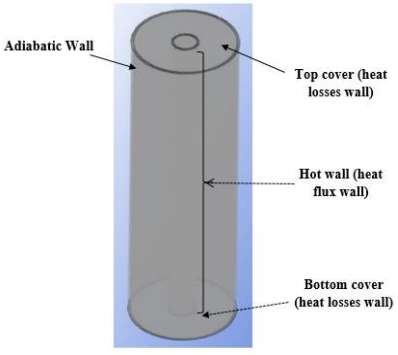

Figure (4) describes the boundary condition on the geometry.

The boundary settings for perfect elements region are given away in table (2).

TABLE 2. EXPLAINS THE BOUNDARY SETTINGS

Boundary/Inlet	
Type	All walls: no slip boundaries (velocity =0).
Boundary / Outlet	
Pressure	0 Pa
Boundary / Wall	
Type	Walls
Adiabatic wall (outermost wall)	Adiabatic
Hot wall (innermost wall, Heat flux wall)	Varies
Walls between the solid domain (stainless steel) and fluid domain (PCM)	Interfaces between the solid domain and fluid domain
The top and bottom covers	Calculated heat losses (calculated heat transfer coefficients from Equation (1))

4. THE GOVERNING EQUATIONS OF THE PROGRAM

ANSYS-CFX software (version 17.0) was used to solve the melting of the PCM. In fact, the melting/solidification model is the enthalpy porosity technique. This technique mainly depends on enthalpy, H, and temperature, T, (Voller and Prakash, 1987).

$$\frac{\partial}{\partial t}(\rho H) + \frac{\partial}{\partial x_i}\left(\rho u_i H - k \frac{\partial T}{\partial x_i}\right) = S \qquad (6)$$

The phase change of PCM usually occurs over a range of temperatures Ts ≤T ≤ Tl. Ts and Tl represent the temperature of the solid phase and liquid phase respectively.

at, Hs ≤H ≤ Hl,

$$T = \beta s\, Ts + \beta l\, Tl \qquad (7)$$

$$\beta l = \frac{H - Hs}{L} \qquad (8)$$

$$\beta l = 1 - \beta s \qquad (9)$$

Where

β= 0, if $T < T_s$

β= 1, if $T > T_l$

$\beta=\frac{T-T_s}{T_l-T_s}$, if ($T_s<T<T_l$)

A mushy zone takes place when both solid and liquid phases coexist. The liquid fraction βl represents the porosity in the mushy zone. Furthermore, there is a resistance term (S) that takes place in the momentum equation (Mat et al., 2013).

A. The continuity equation:

$$\partial_t \rho + \partial_i (\rho u_i) = 0 \quad (10)$$

B. Momentum Equation

$$\frac{\partial}{\partial t}(\rho \vec{u}) + \partial_i(\rho u_i \vec{u}) = \mu \partial_{ii} \vec{u} - \nabla p + \vec{S} \quad (11)$$

Where $\vec{S} = -R \vec{u}$ (12)

In Equation (12), R is the resistance coefficient and can be calculated by Equation (13):

$$R = \frac{(1-\beta)^2}{(\varepsilon+\beta^3)} K^* \quad (13)$$

The value of ε equals 0.001 to avoid dividing by zero when the PCM is in a solid phase. K* has a value in the range of (10^4-10^7 kg/ m3.sec). However, a higher value of K* means a longer time of charging process, (Kheirabadi and Groulx, 2015).

Natural convection has been included in this CFX model by the following equations:

$$\beta l = \min(\max\left(\frac{T-T_s}{T_l-T_s}, 0\right),1) \quad (14)$$

$$\frac{1}{\rho m} = \frac{\beta s}{\rho s} + \frac{\beta l}{\rho l} \quad (15)$$

To include the effect of gravity in our CFX code, we use equation (16) in the momentum equation (11).

$$Fz = -(\rho m - \rho ref)\, g \quad (16)$$

5. SENSITIVITY STUDY

A sensitivity study had been conducted in order to ensure a match between the experimental data and the data from the CFX code. Thermophysical properties of PCM (nitrate binary salt) and nano-PCM (nano-nitrate binary salt) had been either measured or calculated as explained in this section. The values of cp, latent heat, melting temperature, Ts, and liquid Tl had been measured experimentally using the DSC device (Awad, A. et al. 2018a). Laser flash analysis had been used to measure the value of thermal conductivity of PCM and nano-PCM (Awad, A. et al. 2018a). Furthermore, the density of PCM can be calculated according to Equation (17) (Janz et al.,1972)

$\rho = 2064.31 - (4.76248 \times 10^{-4} \times T^2) - (3.36495 \times 10^{-7} \times T^2)$ (17)

The density of nano-PCM can be calculated by equation (18) (Vajjha et al., 2009):

$\rho_{nano\text{-}PCM} = (\varphi n \times \rho_n) + ((1-\varphi_n) \times \rho_{pcm})$ (18)

III. RESULTS AND DISCUSSIONS

The phase change process owns a complex nature. Therefore, an insightful study of the heat transfer of PCM is needed.

In order to improve simulation data, a sensitivity study of thermo-physical properties and mushy zone parameters has been conducted. This would minimize the differences between the experimental data and simulation data.

The latent heat of PCM was measured by (Awad, A. et al. 2018a). We compared the results of five different cases including five different values of latent heat by the CFX. In

figure (5), it is clearly shown that the simulation data of the five different cases of latent heat were not very sensitive in our CFX code. The CFX simulation results of five cases showed minimum differences where value X1 was 1, while X2, X3, X4, and X5 were 1.2, 0.9, 0.7, and 0.5, respectively. In similar, Figure (6) showed that thermal conductivity (k) was not sensitive in CFX code. G1, G2, and G3 were 1, 0.8, and 1.2.

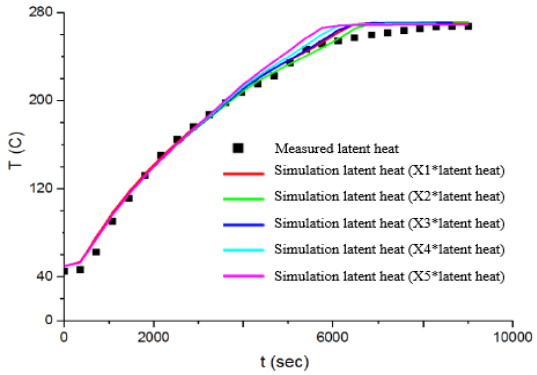

Figure (5) shows the sensitivity results of latent heat.

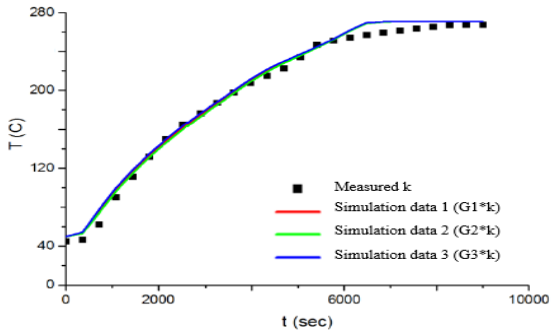

Figure (6) show the sensitivity results of the measured and simulated thermal conductivity.

One of the important parameters was the mushy zone constant. It had been recommended that increasing the values of the mushy zone constant would longer the melting time (Kheirabadi and Groulx, 2015). Because the increases in the mushy zone constant cause an increment in the resistance term and lead to a decrement in the effect of the natural convection. A similar results were concluded, as shown in Figure (7). Simulation data 1 showed the results when the mushy zone constant equals 10^4 kg/m^3.sec. Mushy zone constant can be defined as the measurements of the amplitude of damping (ANSYS Fluent Theory Guide). Furthermore, the mushy zone constant is equal to 10^5 kg/m^3. sec. and 10^6 kg/m^3. sec. for simulation data 2 and simulation data 3, respectively.

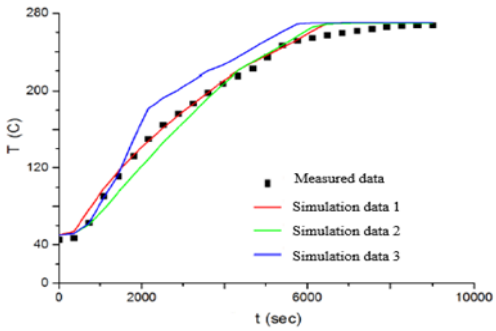

Figure (7) shows the sensitivity study of the mushy zone constant.

After checking the sensitivity of the CFX code, we can see from Figure (8) there is a small differences between the simulation data (CFX data) and the experiment data (experimental data are from experimental rig setup where the paper currently under progress).

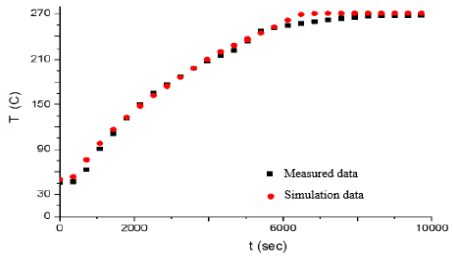

Figure (8) shows the experiment data vs CFX data. These data are for transient temperature measurements at an axial direction of 150 mm.

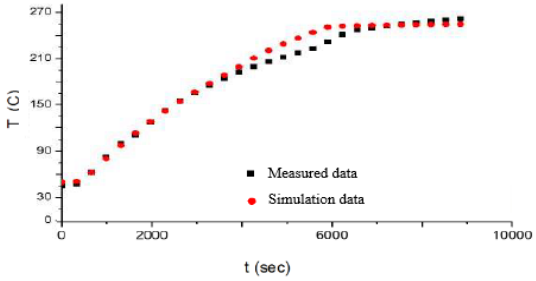

Figure (9) shows the experiment data vs data of CFX code. These data were at the axial direction of 200 mm.

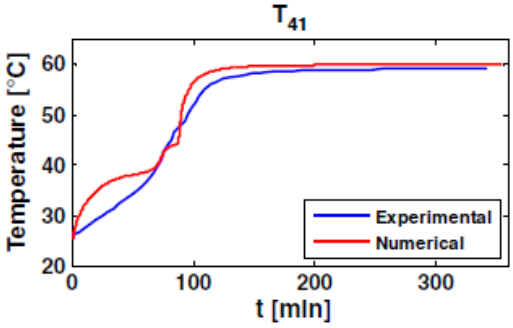

Figure (10) shows the experiment data vs the simulation data (Sciacovelli et al., 2013).

As soon as the PCM starts to melt (around 220 ^{0}C), the heat transfer modes would be a combination of heat transfer by conduction and heat transfer by natural convection due to the phase change of the PCM from solid to liquid. It can be seen the material began to melt faster after the phase change as shown in Figures (8 and 9). Sciacovelli et al., 2013, showed a similar trending between their experimental and simulation data, see Figure (10). Although, they used different type of PCM.

Figures (5-9) shows the data of the storage material (PCM) as nitrate binary salt. As we can see that longer time is required to finish the melting process. Therefore, dispersing nanoparticles into the PCM would faster the charging process as shown in Figure (11). Furthermore, at around 2000 sec, the simulation temperature was 165 ^{0}C for nano-PCM while it was 135 ^{0}C for PCM. Additionally, Figure (12) indicates the liquid mass fraction

comparison between the PCM and nano-PCM. It is clearly shown that nano-PCM would melt faster than the PCM. This means nano-PCM shows an improvement of charging process by 17.021%.

This indicates the advantage of adding nanoparticles into the PCM to improve the heat transfer effects by improving thermophysical properties of the nano-PCM. Because there were an increments in the values of specific heat capacity, thermal conductivity and latent heat of nano-PCM in comparison to PCM without nanoparticles.

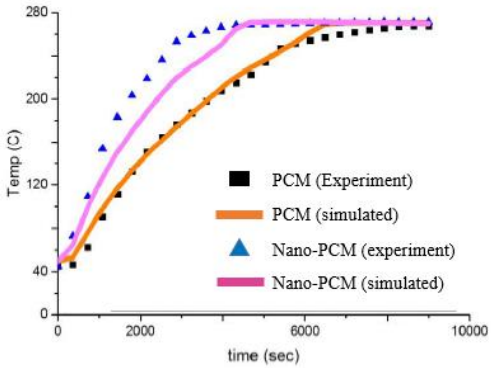

Figure (11) shows the experiment data (Experimental) vs the data from CFX code (Simulated) for PCM and nano-PCM.

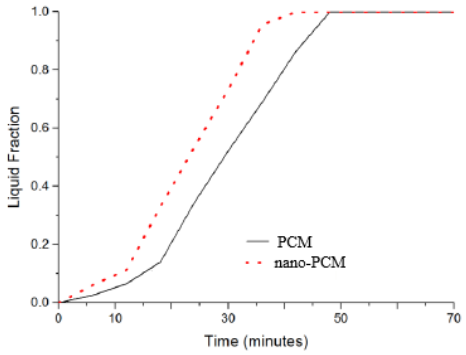

Figure (12) shows the liquid mass fraction of PCM and nano-PCM.

Figure (13) shows the liquid mass fraction comparison between the PCM (to the left) and nano-PCM (to the right). It is clearly shown that nano-PCM would melt faster than PCM. After 1 hour, the phase change of the PCM would start which means the starting of the natural convection. Figure (14) showed the temperature contours after 1 hour. It is obvious the effect of the boussinesq on the temperature distributions. As soon as the phase change starts, then the natural convection effect would directly start.

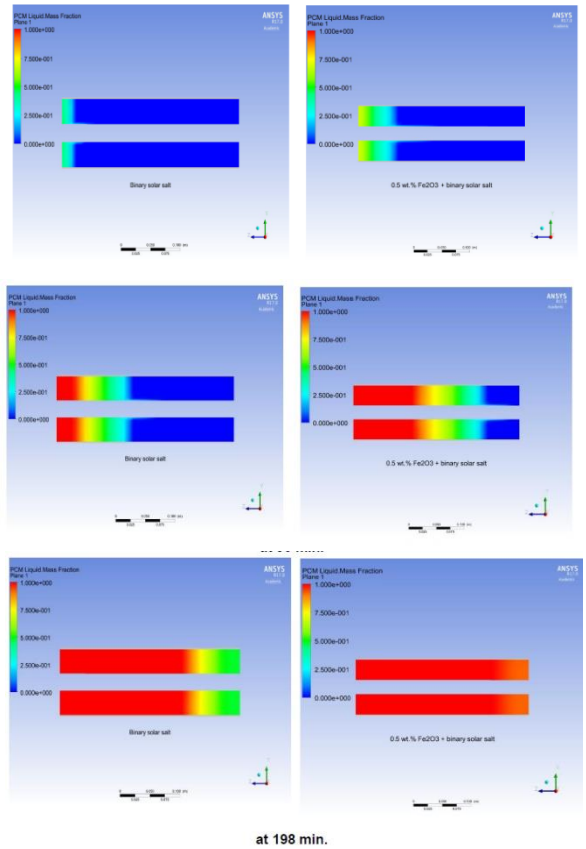

Figure (13) shows the contour of the liquid mass fraction of PCM (to the left) and nano-PCM (to the right) at three selected times.

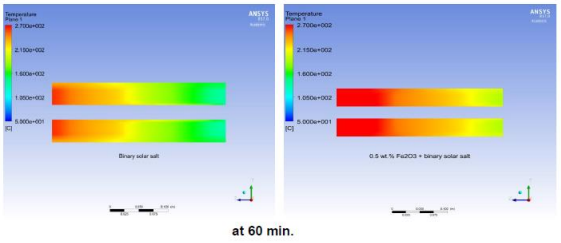

Figure (14) shows the temperature contour of PCM (to the left) and nano-PCM (to the right) after 1 hour.

In total, there is a positive effect of nanoparticles in improving the response of the nanosalt in terms of a faster melting time as well as improving the heat transfer in the storage system in comparison to the solar salt without any additives.

➢ IV. Valdiation of the CFX code

➢ *a. Validation of the CFX code against Fluent code*

The CFX code has been validated against the melting/solidification code in Fluent. This validation is studied in order to check that this CFX is correct to simulate the PCM using the enthalpy porosity model. Figure (15) shows that there is very negligible differences between CFX and Fluent simulations.

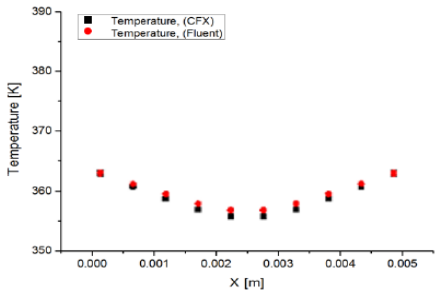

Figure (15) shows data from CFX vs Fluent.

b. Validation of the CFX code against the experimental data According to the sensitivity study, Figures (5-9, 11) showed that there are few differences. The differences between the experiments data and the simulation data could be due to the effect of the following assumptions in the simulation:

- The same densities were assumed for both phases.
- The material is homogenous and isotropic.
- The effect of nanoparticles in the nanosalt samples followed the equations built in the code in the CFX model.

On overall, the differences are acceptable with an acceptable percent of error (less than 5%) between the experiments and the simulation.

V. Conclusion

For the first time, a melting code has been built in the Ansys-CFX. The main conclusions of this study can be divided into:

1. Study the heat transfer of the charging process for the solar energy storage nitrate salt and nano-salt.
2. The CFX code has been validated against the existing melting/solidification code in Ansys-Fluent.
3. Furthermore, CFX code validated against experimental data (paper under progress).
4. The sensitivity study is conducted to indicate the minimum difference between the simulation data and the experimental data.
5. In accordance with the experimental data, the nano-PCM is better in saving the energy with a faster melting process than PCM without any additives.

Therefore, nanosalt could be the new storage material in solar thermal power plants that could save the energy of solar plants.

REFERENCES

1. Ziskind, G., 2021. Modeling of heat transfer in phase change materials for thermal energy storage systems. In Advances in Thermal Energy Storage Systems (pp. 359-379). Woodhead Publishing.
2. Dermardiros, V., Chen, Y. and Athienitis, A.K., 2015. Modelling of an active PCM thermal energy storage for control applications. Energy Procedia, 78, pp.1690-1695.
3. Shmueli, H. et al. 2010. Melting in a vertical cylindrical tube: numerical investigation and comparison with experiments. International Journal of Heat and Mass Transfer. 53(19), pp.4082-4091.
4. Bhaumik, M. 2012. CFD simulation of SDHW Storage Tank with and without Heater. International Journal of Advancements in Research & Technology. 1(2), pp.124-134.
5. Hossain, M.S. et al. 2015. Analysis of Thermal Characteristics of Flared and Rectangular Fin Profiles by Using Finite Element Method.
6. Fadl, M. and Eames, P.C., 2019. Numerical investigation of the influence of mushy zone parameter Amush on heat transfer characteristics in vertically and horizontally oriented thermal energy storage systems. Applied Thermal Engineering, 151, pp.90-99.
7. Yadav, A., Samir, S. and Arıcı, M., 2022. A comprehensive study on melting enhancement by changing tube arrangement in a multi-tube latent heat thermal energy storage system. Journal of Energy Storage, 55, p.105517.
8. Fluent manual Guide-Multiphase Flow Regimes, 2003, Access date [24-10-2022], avialable online: http://www.pmt.usp.br/academic/martoran/notasmodelosgrad/ANSYS%20Fluent%20Users%20Guide.pdf
9. Sebti, S. et al. 2011. A numerical investigation of solidification in horizontal concentric annuli filled with nano-enhanced phase change material (NEPCM). World Applied Sciences Journal. 13(1), pp.09-15
10. Valan, A.A. et al. 2013. Numerical performance study of paraffin wax dispersed with alumina in a concentric pipe latent heat storage system. *Thermal science.* **17**(2), pp.419-430.
11. Sharma, R. et al. 2014. Numerical study for enhancement of solidification of phase change materials using trapezoidal cavity. Powder Technology. 268, pp.38-47.
12. Li, Z., Shahsavar, A., Al-Rashed, A.A. and Talebizadehsardari, P., 2020. Effect of porous medium and nanoparticles presences in a counter-current triple-tube composite porous/nano-PCM system. Applied Thermal Engineering, 167, p.114777.
13. Bouzennada, T., Mechighel, F., Ghachem, K. and Kolsi, L., 2021. Numerical Simulation of the Impact of the Heat Source Position on Melting of a Nano-Enhanced Phase Change Material. Nanomaterials, 11(6), p.1425.
14. Ahmed, S., Abderrahmane, A., Saeed, A.M., Guedri, K., Mourad, A., Younis, O., Botmart, T. and Shah, N.A., 2022. Melting enhancement of PCM in a finned tube latent heat thermal energy storage. Scientific Reports, 12(1), pp.1-14.
15. Abderrahmane, A., Qasem, N.A., Mourad, A., Al-Khaleel, M., Said, Z., Guedri, K., Younis, O. and Marzouki, R., 2022. Enhancing the melting process of shell-and-tube PCM thermal energy storage unit using modified tube design. Nanomaterials, 12(17), p.3078.
16. Bakker, A. 2002. Lecture 7 – Meshing, Applied Computational Fluid Dynamics.
17. Tay, N. et al. 2015. Investigation of the effect of dynamic melting in a tube-in-tank PCM system using a CFD model. Applied Energy. 137, pp.738-747.
18. Thirumaleshwar, M. 2009. *Fundamentals of heat and mass transfer.* Pearson Education India.
19. Voller, V.R. and Prakash, C. 1987. A fixed grid numerical modlling methodology for convection-diffusion mushy region phase-change problems *International Journal Heat Mass Transfer.* **30**(8), pp.1709-1719.

20. Mat, S. et al. 2013. Enhance heat transfer for PCM melting in triplex tube with internal–external fins. *Energy Conversion and Management.* **74**, pp.223-236.

Symbol	Definition	Symbol	Definition

21. Kheirabadi, A.C. and Groulx, D. 2015. The effect of the mushy-zone constant on simulated phase change heat transfer. In: *ICHMT DIGITAL LIBRARY ONLINE*: Begel House Inc.

22. Awad, A. et al. 2018a. Thermal-physical properties of nanoparticle-seeded nitrate molten salts. *Renewable Energy.* **120**, pp.275-288.

23. Janz, G. et al. 1972. Molten salts: Volume 3 nitrates, nitrites, and mixtures: Electrical conductance, density, viscosity, and surface tension data. *Journal of Physical and Chemical Reference Data.* **1**(3), pp.581-746.

24. Vajjha, R. et al. 2009. Density measurement of different nanofluids and their comparison with theory. *Petroleum Science and Technology.* **27**(6), pp.612-624.

25. Fluent manual Guide-Multiphase Flow Regimes, 2003, Access date [31-12-2022], available online: http://www.pmt.usp.br/academic/martoran/notasmodelosgrad/ANSYS%20Fluent%20Theory%20Guide%2015.pdf

26. Sciacovelli, A. et al. 2013. Melting of PCM in a thermal energy storage unit: Numerical investigation and effect of nanoparticle enhancement. International Journal of Energy Research. 37(13), pp.1610-1623.

h	Heat transfer coefficient, W/ (m^2. K).	ρm	The density of the mixture, kg/m^3
Nu	Nusselt number	ρref	Reference density, kg/m^3
k	Thermal conductivity, W/(m. K)	$\rho_{nano\text{-}PCM}$	The density of the nano-PCM, kg/m^3
Lc	Characteristic length, m	φ_n	concentration of nanoparticles
Ra	Rayleigh number	ρ_n	density of nanoparticles, kg/m^3
ρ	Density, kg/m^3	ρ_{pcm}	density of PCM, kg/m^3
g	Gravity, m/ sec^2		
B	Thermal expansion coefficient	cp	Specific heat capacity, J/ (g. K)
Ts	Surface temperature, ^{0}C	ΔT or dT	Temperature differences, K
T∞	Ambient temperature, ^{0}C	Tl	The temperature of the liquid phase, K
Pr	Prandtal number	T	Temperature, K
μ	Viscosity		
Tf	Film temperature, ^{0}C	ρm	The density of the mixture, kg/m^3
H	specific enthalpy (J/kg)	ρref	Reference density, kg/m^3
Hs	specific enthalpy of solid phase(J/kg)	Fz	Gravity force, N
Hl	specific enthalpy of liquid phase (J/kg)	$\rho_{nano\text{-}PCM}$	The density of the nano-PCM, kg/m^3
u*i*	u*i* is the velocity (m/s),	ρref	Reference density, kg/m^3
S	heat source and sink per unit volume (W/m^3).	Fz	Gravity force, N
βs	Solid phase mass fraction	R	resistance coefficient, kg/ m3.sec
Ts	The temperature of the solid phase, K	ρs	The density of solid phase, kg/m^3
		ρl	The density of liquid phase, kg/m^3
βl	liquid phase mass fraction	L	Latent heat, J/kg

Nomenclature: